# Lattice models for Josephson junctions and graphene superlattices

Ostroukh, V.

# Chapter 3

# $h/e$ superconducting quantum interference through trivial edge states in InAs

## 3.1 Introduction

Topological systems are a hot topic in condensed matter physics [51]. This is largely motivated by the existence of states at the interface between two topologically distinct phases, for example helical edge states in a quantum spin Hall insulator (QSHI) [52, 53]. Inducing superconductivity in these edge states would form a topological superconductor [51]. Superconducting edge transport has already been found in materials that are predicted to be QSHI [19, 32]. However, edge states can also have a non-topological origin. Trivial edge conduction is found in InAs alongside the chiral edge states in the QH regime [54] and recently in the proposed QSHI InAs/GaSb as well [55, 56]. To be able to discriminate between topological and trivial states it is crucial to study transport through triv-

The contents of this chapter have been published and reprinted with permission from F. K. de Vries, T. Timmerman, V. P. Ostroukh, J. van Veen *et. al.*, Phys. Rev. Lett. **120**, 047702 (2018). 

ial edges also and clarify differences and similarities between them. In this work we study the superconducting transport through trivial edge states in non-topological InAs Josephson junctions using superconducting quantum interference (SQI) measurements. We find supercurrent carried by these edge states and an intriguing $h/e$ periodic signal in a superconducting quantum interference device (SQUID) geometry.

## 3.2 Description of the experiment

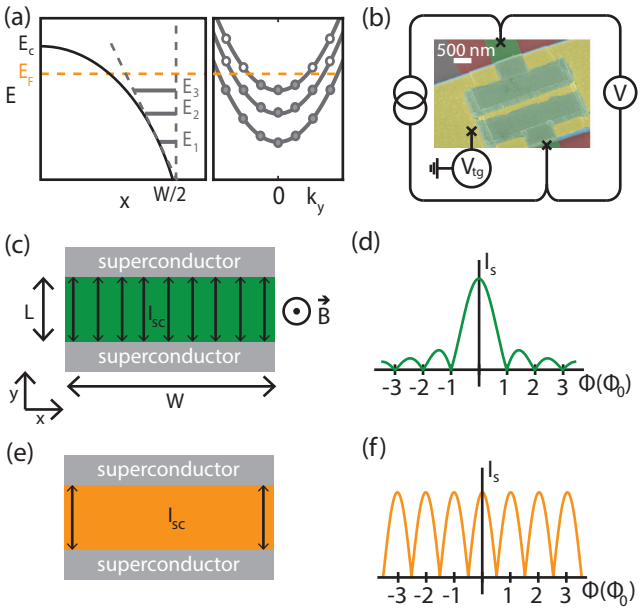


**Figure 3.1.** (a) Sketch of the conduction band minimum around the edge of a 2DEG with Fermi level pinning at $W/2$. The band bending leads to a roughly triangular quantum well in the vicinity of the edge, therefore one-dimensional sub bands form of which three are drawn, as an example. The orange dashed line indicates the Fermi level corresponding to the current distribution in (e). (b) False coloured SEM image of the device with dimensions $W = 4$ µm and $L = 500$ nm, where the quasi-four terminal measurement setup is added. Red is the mesa, green the NbTiN contacts, blue $SiN_x$ dielectric and yellow the gold top gate. (c) Schematic representation of a Josephson junction of width $W$ and length $L$. A homogeneously distributed supercurrent $I_{sc}$ is running through the whole junction, resulting in (d) a Fraunhofer SQI pattern. (e) If supercurrent only flows along the edges of the sample, (f) a SQUID pattern is observed.

Trivial edge states arise when the Fermi level resides in the band gap in the bulk, while being pinned in the conduction band at the surface. Then, band bending leads to electron accumulation at that surface as schematically drawn in Fig. 1(a). The Fermi level pinning can have several origins: truncating the Bloch functions in space [57, 58], a work function difference [59], the built-in electric field in a heterostack [60] and the surface termination [61]. In our 2D InAs Josephson junctions the accumulation surface is located at the edge of the mesa that is defined by wet etching. The quantum well is MBE grown on a GaSb substrate serving as a global bottom gate. The superconducting electrodes are made of sputtered NbTiN with a spacing of 500 nm and a width of 4 µm. A $SiN_x$ dielectric separates the top gate from the heterostructure. Electrical quasi-four terminal measurements [see Fig.1(b)] are performed in a dilution refrigerator with an electron temperature of 60 mK unless stated otherwise.

The electron density in the InAs quantum well is altered by using the electrostatic gates, $V_{tg}$ and $V_{bg}$, located above and below the 2DEG. Decreasing the density subsequently increases the normal state resistance $R_n$ and reduces the switching current $I_s$ as shown in Fig. 2(a). The Josephson junction is first characterized at $V_{tg} = 0$ V and $V_{bg}$ = -1.65 V, where the largest switching current is observed. From the IV trace in Fig. 2(a) we estimate an induced superconducting gap of 0.4 meV and, using the corrected OBTK model [62], a transmission of $T = 0.73$. The junction is quasi-ballistic because the mean free path of 2.8 µm (extracted from a Hall bar device on the same wafer) is larger than its length $L$ of 500 nm. The large superconducting gap and high transmission value indicate a high quality InAs Josephson junction.

## 3.3 Superconducting quantum interference measurements

SQI measurements have successfully been used before to gather information on the supercurrent density profile in Josephson junctions [19, 32, 63]. This is typically done, using Dynes-Fulton approach [11], which connects critical current dependency on magnetic field $I_c(B)$ and zero-field supercurrent density profile $j(x)$ with a Fourier transform. It was originally developed for tunnel junctions, but can also be applied to transparent junctions under several assumptions. Firstly, we should have a sinusoidal current-phase dependency, which is in accordance with the transmission

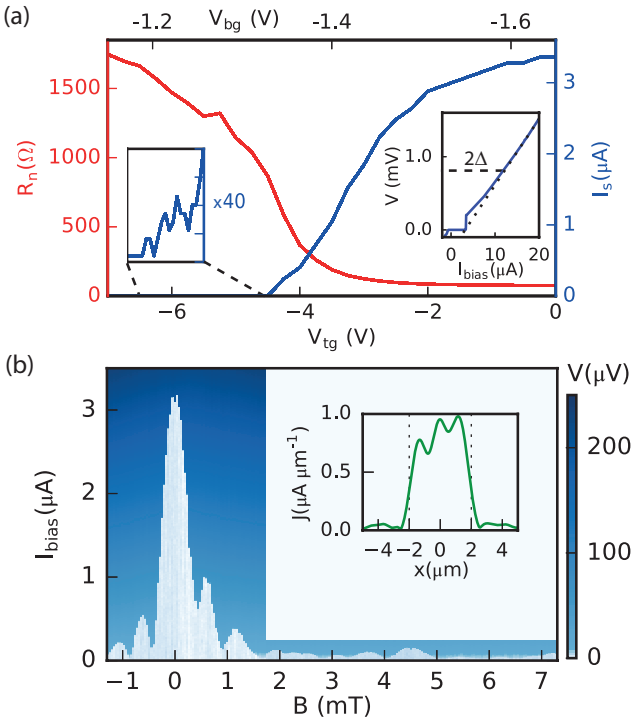


**Figure 3.2.** (a) Normal state resistance $R_n$ and switching current $I_s$ at the respective top gate $V_{tg}$ and bottom gate $V_{bg}$ voltages. The left inset depicts a seperate measurement at the indicated gate voltages, where a smaller current bias step size is used for higher resolution. The right inset shows an IV trace at $V_{tg} = 0$ V and $V_{bg} =$ -1.65 V , where two dashed lines are added for extraction of the induced superconducting gap $\Delta$ and the excess current. (b) The measured voltage as function of the applied current $I_{bias}$ and perpendicular magnetic field $B$ at $V_{tg} = 0$ V and $V_{bg} =$ -1.65 V. The inset depicts the calculated supercurrent density along the width of the device that is indicated by the dotted lines.

value and temperature in our experiment [64]. Secondly, the Andreev levels, that carry supercurrent in the junction, may only weakly deviate from the longitudinal propagation. Our junction satisfies this constraint since the superconducting coherence length $\zeta = \hbar v_F/\Delta \approx 1.3$ µm $> L$ [34]. If both assumptions hold, we expect Fraunhofer SQI pattern in the case of homogeneous current distribution (Fig. 1(c-d)) and SQUID pattern in the case of current flowing along the edges (Fig. 1(e-f)).

A SQI measurement at the largest switching current reveals a Fraun-

hofer like pattern as shown in Fig. 2(b). The central lobe is twice as wide as the side lobes and the amplitude decreases as expected. The slight asymmetry in the amplitudes we contribute to breaking of the mirror symmetry of the sample in the direction along the current [65]. The effective length of the junction [$\lambda = \delta B_{lobe}/(\Phi_0 \cdot W)$] of 1.2 µm is extracted from the periodicity of the SQI pattern. Flux focusing due to the Meissner effect causes it to be larger than the junction length ($\lambda > L$) [66]. The extracted current density profile, plotted in Fig. 2(b), is close to uniform. The supercurrent is thus dominated by bulk transport as expected at these gate voltages.

The interference pattern in Fig. 2(b) deviates from the expected pattern after the second lobe. Recently a similar distorted Fraunhofer tail was observed and discussed in graphene [67]. The perpendicular magnetic field exerts a Lorentz force on the electron and holes suppressing the formation of Andreev bound states. The suppression becomes relevant at a magnetic field scale of $\Delta/eLv_F$, equal to 1 mT in our case, roughly agreeing with the observation. The analysis only holds for the bulk of the junction, since the scattering at the edges reduces the difference in the electron and hole motion in a magnetic field.

Next we study the SQI pattern as the Fermi level is decreased by tuning the top gate to more negative values. The upper two (green) traces in Fig. 3(a) have a wide central lobe, identifying a Fraunhofer pattern. The effective length is $\lambda$ =1.7 µm, different from before, which we believe is due to different vortex pinning because of the larger magnetic field range of the measurement. In the third (first blue) trace we observe that the first nodes turn into peaks, which is highlighted by the dashed lines. This is the transition from a Fraunhofer to a SQUID pattern. Curiously the amplitude and width of the peaks are alternating in the blue traces in Fig. 3(a). The even-odd pattern is composed of an $h/e$ and $h/2e$ periodic signal. An even-odd pattern was observed before in Pribiag *et al.* [19]. In comparison, in this work the amplitude difference in the lobes is much larger and the pattern is visible over a large gate range. The calculated supercurrent density profiles in Fig. 3(b) have a central peak that is physically unlikely considering the device geometry. The cause of this intriging interference pattern will be discussed in more detail later. Reducing $V_{tg}$ further we find a clear $h/2e$ periodic SQUID interference pattern in the bottom two (orange) traces. This is a strong indication of edge conduction in our device. Confirmed by the edge transport only in the extracted supercurrent den-

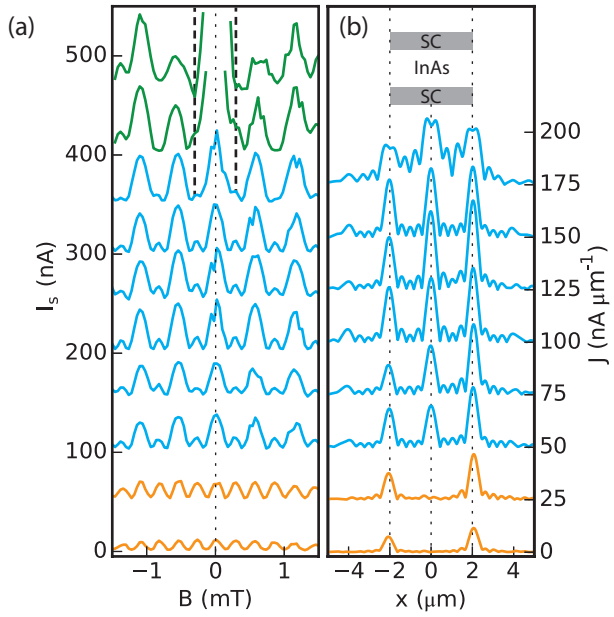


**Figure 3.3.** (a) The switching current plotted as function of perpendicular magnetic field and (b) the corresponding current density along the width of the device (see inset), assuming the validity of the Dynes-Fulton approach. The gate values used are from bottom to top: $V_{tg}$ -5.4 V to -3.6 V (0.2 V step) and $V_{bg}$ -1.270 V to -1.396 V (0.014 V step). The green, blue and orange traces are Fraunhofer, even-odd and SQUID patterns, respectively. Since the current is only swept up to 100 nA, the green traces are not suitable for extracting a supercurrent density profile. The traces are offset by 50 nA in (a) and 25 nA/μm in (b).

sity profiles in Fig. 3(b). The transition from bulk to edge transport as a function of gate voltage is measured in several other Josephson junctions. Since we observe supercurrent through the trivial edge states of an InAs quantum well, we conclude that a clear demonstration of superconducting edges alone does not prove induced superconductivity in topological edge states.

## 3.4 Even-odd SQI pattern

We now return to the remarkable $h/e$ SQUID signal to investigate its origin. Figure 4(a) shows a more detailed measurement in this gate regime,

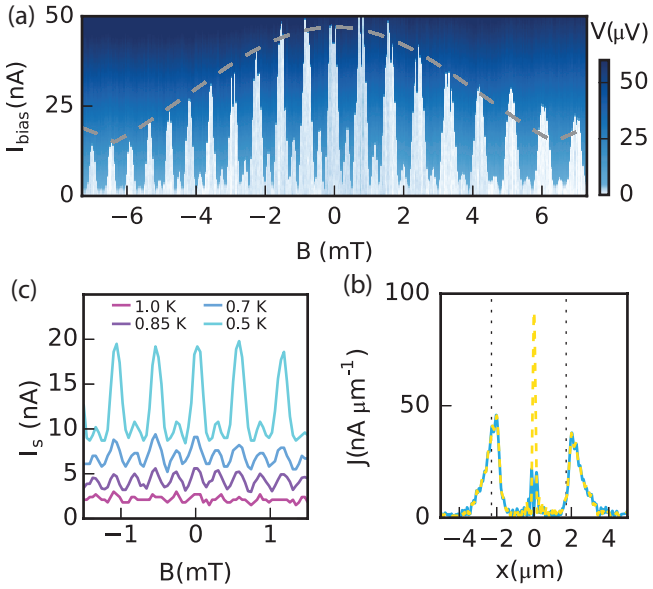


**Figure 3.4.** (a) Measured voltage as a function of $I_{bias}$ and magnetic field $B$ at $V_{tg}$ = -5 V and $V_{bg}$ = -1.29 V. (b) Switching current versus the magnetic field for different temperatures at the same gate voltages as (a). The traces are offset by 5 nA for clarity. (c) Current density profile, calculated from the SQI pattern of (a). The blue trace uses equation (1), thus correcting the vertical offset in the SQI pattern. The yellow dashed trace is extracted without this correction.

the even-odd pattern is observed over more than 25 oscillations. The envelope of the peaks is attributed to the finite width of the edge channels. The effect is suppressed by raising the temperature [see Fig. 4(b)], for $T >$ 850 mK a regular $h/2e$ SQUID pattern remains. The origin can not lie in effects that occur beyond a certain critical magnetic field, like $0 - \pi$ transitions [68], edge effects [43, 69] and a topological state, because we observe the even-odd pattern around zero magnetic field as well. An effect that does not rely on magnetic field and is strongly temperature dependent is crossed Andreev reflection [70].

The lowest order crossed Andreev reflection (up to electron-hole symmetry) is schematically depicted in Fig. 5(a). An electron travels along one edge, whereafter a hole is retroreflected over the other edge. This process alone is independent of the flux through the junction, but still adds to the critical current (see Sec. 2.5). Higher order processes that include an electron that encircles the junction completely pick up an $h/e$

phase when a flux quantum threads through the junction, hence the supercurrent becomes $h/e$ periodic [71]. Additionaly, interference processes between crossed Andreev and single edge Andreev states could lead to a $h/e$ contribution [72]. It is important to note that the critical current is $h/e$ periodic in flux trough the sample, but still $2\pi$ periodic in superconducting phase difference.

Forming crossed Andreev states in the junction is only possible if the particles can flow along the contacts. Electrostatic simulations indeed show a large electron density close to the contacts at gate voltages where the bulk is already depleted, because of local screening of the top gate. Nevertheless the needed coherence length for a crossed Andreev reflection is on the order of 10 µm, where the estimated superconducting coherence length (from bulk values) is 1.3 µm. The difference between these values remains an open question.

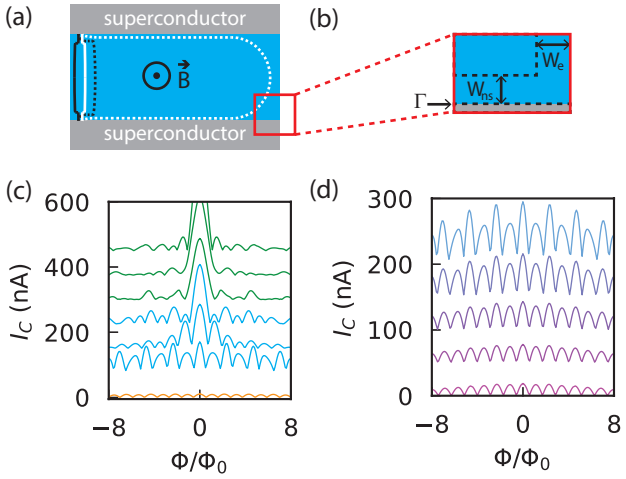


**Figure 3.5.** (a) Schematic representation of two crossed Andreev processes. The black and white lines indicate electron and hole trajectories or vice versa. The solid lines represent a single edge Andreev state and the dotted lines a crossed Andreev state. (b) Detailed sketch of one corner of junction in our tight binding mode indicating the widths $W_{ns}$ and $W_e$, and tunnel barrier $\Gamma$. (c) Calculated SQI patterns at overall chemical potential ranging from -0.06 eV to 0.18 eV (0.04 eV step) at 0.46 K and (d) at temperatures 0.4 K, 0.9 K, 1.4 K, 1.9 K, 2.3 K at a chemical potential of -0.2 eV. Traces are offset by 10 nA for clarity. In (c) the color represents the type of interference pattern, green for Fraunhofer, blue for even-odd and orange for SQUID, respectively.

## 3.5 Phenomenological model: crossed Andreev reflection impact

The phenomenological model proposed in Chapter 2 considers both single edge and crossed Andreev states. In our device we expect the lowest order crossed Andreev states to contribute most because of the short coherence length. Combining their flux insensitive contribution to the critical current and the usual $h/2e$ periodic contribution from single edge Andreev bound states, the model predicts an even-odd or $h/e$ SQUID pattern:

$$I_c(\Phi) = I_0 \left|\cos(\pi\Phi/\Phi_0) + f\right|. \tag{3.1}$$

Where $I_0$ the critical field at zero magnetic field and $\Phi$ is the applied flux. Constant $f$ can be arbitrarily large, it dependes on the ratio $\Gamma$ between the probability to Andreev reflect on a node versus the probability to scatter to another edge and is exponentially suppressed by the width of the sample:

$$f \sim \Gamma^{-1} \frac{k_B T}{\Delta} e^{-2\pi(k_B T/\Delta)(W/\zeta)}. \tag{3.2}$$

The predicted pattern is thus the absolute value of a vertically offsetted cosine function. That is exactly the pattern we measured in Fig. 3(a) and 4(a) as both the amplitude and width of the lobes alternate From the data we estimate $f = 0.3$ and, using the other known parameters, find $\Gamma \sim 10^{-1}$. Taking the Fourier transform in the Dynes-Fulton analysis, offset $f$ leads to a non-physical current density around zero, like we observe in the current density profiles in Fig. 3(b) and the yellow dashed line in Fig. 4(c). Moreover, the Dynes-Fulton approach is not valid here since crossed Andreev reflection does not meet the second assumption of having straight trajectories only. We can compensate the crossed Andreev contribution by subtracting the constant offset of $f \cdot I_0$=11 nA. This results in a current distribution with mainly current along the edges, as plotted in the blue trace of Fig. 4(c). We did not take into account that $I_0$ is actually not constant due to the Fraunhofer envelope of the SQI pattern, so the current density in the center of the junction is not entirely eliminated.

## 3.6 Tight-binding simulations

Even though the SQI pattern from the phenomenological model is in qualitative agreement with our data, we also present a tight binding model of

system in order to connect it directly to experimentally accessible parameters. In the microscopic model we include the superconducting gap as measured, the width of the paths along the contacts $W_{ns}$ of 20 nm [extracted from the Fraunhofer envelope in Fig. 4(a)], and Fermi level pinning on the edges leading to edge current in the region $W_e$. It is crucial to also take into account a tunnel barrier $\Gamma$ at the contacts that has a magnitude consistent with the measured transmission value. This barrier enhances normal reflection and therefore elongates the length electrons and holes travel before Andreev reflecting. Incorporating these experimental values we find an $h/e$ SQUID pattern. Emulating the experimental gating effect by changing the overall chemical potential results in a crossover from even-odd to Fraunhofer [Fig. 5(c)], consistent with the measurement in Fig. 3. As a check, $W_{ns}$ is reduced in steps to zero, which results in a SQUID pattern. Additionally, in Fig. 5(d) we observe that increasing the temperature indeed smears out the even-odd pattern and leaves us with a regular SQUID pattern, similar to the experimental data in Fig. 4(b). Summarizing, both the phenomenological model and the microscopic model support our hypothesis of the $h/e$ SQUID originating from crossed Andreev states.

## 3.7 Conclusion

We have experimentally shown that trivial edge states can support highly coherent superconducting transport that also becomes visible in an $h/e$ periodic SQI pattern. Both effects have been considered as possible signatures for inducing superconductivity in topological edge states before [19, 32]. Therefore we conclude that superconducting edge transport and an $h/e$ SQUID pattern only, cannot distinguish between topological and trivial edge states, nor can it be considered a definite proof for a topological phase.

## 3.8 Appendix

### 3.8.1 Tight binding model

We have taken the following Hamiltonian for tight binding simulations:

$$H = \left( \frac{\hbar^2(k_x^2 + k_y^2)}{2m_{\text{eff}}} - \mu(x,y) \right) \tau_z + \alpha(k_x\sigma_y - k_y\sigma_x)\tau_z + g\mu_{\text{B}}B(x)\sigma_z + \Delta(x)\tau_x, \tag{3.3}$$

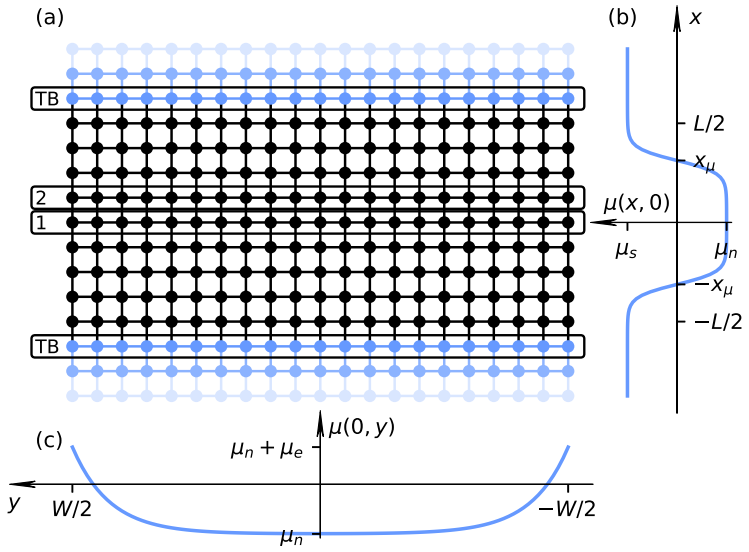


**Figure 3.6.** (a) Schematical representation of a tight-binding model. Bogolyubov-de Gennes Hamiltonian is discretized on a square lattice. Superconducting sites of the system have a blue color, normal – black. A tunnel barrier is created, using one row of sites with decreased chemical potential (marked TB on the scheme). The current was calculated from Green's function of sites, marked 1 and 2 on the scheme (see the detailed explanation below). (b) Chemical potential profile for $x = 0$. Offset between location of chemical potential step and superconducting region together with the tunnel barrier leads to formation of scattering channel between edges. (c) Chemical potential profile for $y = 0$. Band bending is represented with an increased chemical potential at the edges, leading to edge conductivity in a doped regime.

where $\sigma$ Pauli matrices correspond to the spin degree of freedom, and $\tau$ – to the electron and hole one. It is discretized on a square lattice with lattice constant $a = 2$ nm. The normal part of a SNS junction is represented as a rectangle $-L/2 \leq x \leq L/2$ and $-W/2 \leq y \leq W/2$, the superconducting parts – as translationally invariant in $x$ direction stripes with $-W/2 \leq y \leq W/2$. Proximity-induced pairing potential $\Delta(x)$ is zero in a normal part and constant in a superconducting part of the system, with a step-like transition. The magnetic field is assumed to be fully

screened by the superconductors. Its impact is included as Zeeman term and via Peierls substitution.

At first realistic values of $\alpha = 5 \cdot 10^{-12}\,\mathrm{eV} \cdot \mathrm{m}$ and $g = 11.5$ for the Rashba and Zeeman term were used to verify that they do not play an important role in this parameter regime. After we were sure that Zeeman and Rashba terms can be neglected, we have put $\alpha = 0$ and $g = 0$ for the sake of numerical performance. This allowed to decouple spins and decrease the dimensionality of the Hamiltonian twice, since both decoupled subblocks contribute equally to the current.

Chemical potential $\mu(x, y)$ is selected to capture primary features of the device: band bending near the edges and screening near the NS boundaries top gate. It has the following form:

$$\mu(x,y) = \frac{\mu_{\mathrm{norm}} + \delta\mu_{\mathrm{edge}}(y)}{2}\left(\tanh\frac{x+x_\mu}{\lambda_\mu} - \tanh\frac{x-x_\mu}{\lambda_\mu}\right) + \frac{\mu_{\mathrm{sc}}}{2}\left(2 - \tanh\frac{x+x_\mu}{\lambda_\mu} + \tanh\frac{x-x_\mu}{\lambda_\mu}\right), \tag{3.4}$$

where

$$\delta\mu_{\mathrm{edge}}(y) = 2\mu_{\mathrm{e}} e^{-W/2\lambda_e}\cosh\frac{y}{\lambda_e} \tag{3.5}$$

is the term, that introduces band bending near the edges of a normal part. $\mu_{\mathrm{norm}}$ and $\mu_{\mathrm{sc}}$ are chemical potentials in gated area (primarily normal part) and area screened by the superconducting contacts. If normal part is governed to the insulating state with negative $\mu_{\mathrm{norm}}$, the offset between $L/2$ and $x_\mu$ leads to formation of a conducting channel on the NS boundaries of the junction, with a width:

$$W_{\mathrm{ns}} = L/2 - x_\mu. \tag{3.6}$$

The tunnel barrier on the NS interface was represented as a single row of sites with a chemical potential reduced by $\Delta\mu_{\mathrm{TB}}$.

The finite-temperature critical current of the SNS junction was calculated by maximizing the current-phase dependency, similarly to the approach, used in [73]. The Green's function was numerically calculated for several Matsubara frequencies on two neighbouring rows of the sites in the normal part of the junction, then the current was obtained by the summation:

$$I = \frac{2ek_BT}{\hbar}\sum_{n=0}^{N_{\max}}\left(\Im\,\mathrm{tr}\,H_{21}G_{12}(i\omega_n) - \Im\,\mathrm{tr}\,H_{12}G_{21}(i\omega_n)\right). \tag{3.7}$$

Here $H_{21}$ and $G_{21}$ denote hopping matrix and Green's function subblock from cells of row 1 to row 2, indicated on Fig. 3.6 (all the hoppings, that form a cut through the system), and vice versa. $\omega_n = (2n+1)\pi k_B T$ is the $n$-th Matsubara frequency. Value $N_{\max}$ was obtained dynamically, based on the estimated convergence rate. The Green's functions were calculated, using package Kwant [16].

The numerical values of parameters, used for simulations, are presented in Table 3.1. A lattice constant of $a = 2$ nm was selected small enough to capture characteristic length scales of an edge and NS boundary current channels.

| $W$ [nm] | $L$ [nm] | $\lambda_e$ [nm] | $\lambda_\mu$ [nm] | $x_\mu$ [nm] |
|---|---|---|---|---|
| 400 | 200 | 28 | 1 | $0 \div 50$ |

| $m_{\text{eff}}/m_e$ | $\Delta$ [eV] | $\mu_{sc}$ [eV] | $\delta\mu_e$ [eV] |
|---|---|---|---|
| 0.04 | $4 \cdot 10^{-4}$ | 0.2 | 0.15 |

**Table 3.1.** Numerical parameters, used for tight-binding simulations.

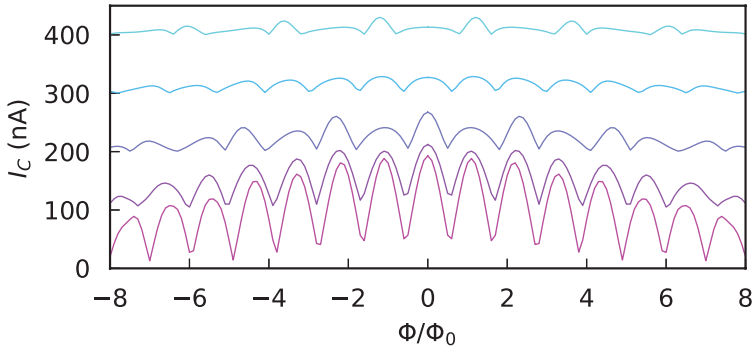


**Figure 3.7.** Tight binding calculation of the superconducting quantum interference as a function of tunnel barrier strength at the contact. Increasing the tunnel barrier height leads to enhanced normal reflection with respect to Andreev reflection. The electrons or holes then have a higher chance of traversing along the contact before Andreev reflecting. Forming a crossed Andreev states requires the charge carriers to traverse around the junction fully. Therefore enhanced normal reflection is benefecial for forming these states and the resulting even-odd SQI pattern. Here we plot the SQI patterns for a tunnel barrier strength ranging from 0.6 eV to 1.40 eV (bottom to top) in 0.2 eV steps.

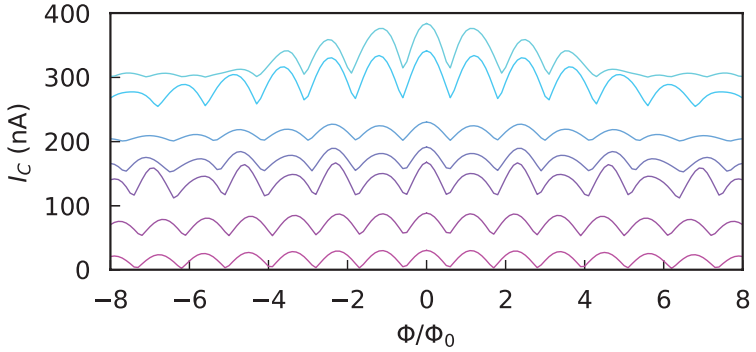


**Figure 3.8.** Tight binding calculation of the superconducting quantum interference as a function of width of the channel along the edge. As a sanity check: if the width is 2 nm (bottom trace), we do not see even-odd effect. Increasing the width (in 8 nm steps up to 50 nm), increases the number of channels along the contact and the coherence length, up to the point that the 1D channel become 2D and the even-odd effect reduces again.